

Run-to-tumble variability controls the surface residence times of *E. coli* bacteria

Gaspard Junot¹, Thierry Darnige¹, Anke Lindner¹, Vincent A. Martinez³
Jochen Arlt³, Angela Dawson³, Wilson C. K. Poon³, Harold Auradou², Eric Clément^{4,1}

¹Laboratoire PMMH-ESPCI Paris, PSL Research University,
Sorbonne Université and Denis Diderot, 7, quai Saint-Bernard, Paris, France.

² Université Paris-Saclay, CNRS, FAST, 91405, Orsay, France.

³SUPA and the School of Physics & Astronomy, The University of Edinburgh,
Peter Guthrie Tait Road, Edinburgh EH9 3FD, United Kingdom.

⁴Institut Universitaire de France (IUF).

(Dated: July 26, 2021)

Motile bacteria are known to accumulate at surfaces, eventually leading to changes in bacterial motility and bio-film formation. Using a novel two-colour, three-dimensional Lagrangian tracking technique, following simultaneously the body and flagella of wild-type *Escherichia coli*, we observe long surface residence times and monitor escapes correspond mostly to immediately antecedent tumbling events. Modelling the motility accounting for a large behavioural variability in run-times, reproduces all experimental findings and gives new insights into surface trapping efficiency.

Suspensions of ‘active’, or self-propelled, particles such as motile microorganisms display rich, often counter-intuitive, phenomena not seen in suspensions of passive colloids [1]. For example, a bulk suspension of motile bacteria can display a viscosity lower than that of the pure solvent [2, 3]. On the other hand, it is long known that motile bacteria accumulate at walls [4–6]. Persistence in the swimming direction along surfaces is a generic contributing factor to such surface ‘trapping’ effect, with hydrodynamics or eventually transient adhesion [7], playing a details-dependent role.

Bacterial surface motility is implicated in many industrial, biomedical or environmental issues, such as bacterial contamination or biofouling [8, 9]. The attachment of bacteria to surfaces often leads to the build up of hard-to-eradicate biofilms and is problematic in a wide range of areas, including medical implants[10], water purification systems[11], and industrial processes[12]. The biofouling of metal ship hulls frequently proceeds with bacterial adhesion before progressing to larger marine organisms[8, 9]. In natural processes, the attachment of bacteria to roots constitutes the first physical step in many plant–microbe interactions[13]. Adhesion can originate with surface restriction to flagellar motion [14] triggering downstream events such as the secretion of polysaccharides for structuring mature biofilms[15]. The initial stage that precedes surface adhesion is therefore the ‘residence time’ τ of a swimming bacterium on the surface, which depends on how the swimmer loses directional memory [7]. This quantity is also key to various statistical modelling designed to understand the problem of large scale bacterial transport in various environmental or bio-medical situations.

Wild-type (WT) *Escherichia coli* performs run and tumble (R&T), in which approximately straight runs are interspersed with rapid tumbles where the swimming direction changes rapidly and more or less randomly. In smooth-swimming mutants, tumbling is heav-

ily suppressed, and reorientation is predominantly due to rotational diffusion. How rotational diffusion reorients near-wall bacteria to allow escape from surface trapping is reasonably well understood [5, 16]. The mechanism in wild-type R&T organisms is much more complex [17, 18]. To date, the detailed micro-hydrodynamics of this phenomenon remains a challenge even for state-of-the-art numerics [19]. Experimental data from Molaie et al. [20] using digital holographic microscopy to capture 3D trajectories of wild-type *E. coli* near a solid surface suggest that surfaces inhibit tumbling and polarise the post-tumbling direction parallel to the surface, so that tumbling is not a particularly effective escaping mechanism. In this study, individual motile *E. coli* bacteria were tracked one by one using two-colour three-dimensional tracking (2C-3DT) to provide with an unprecedented precision their R&T statistics. Observations of their displacement close to a surface were made during long period of times allowing to obtain for the first time the surface residence time distribution, the angular distributions for arrival and escape, and the tumbling time distributions at the surface. Those distributions were compared with measurements performed with the same technique but away from the surface. We find long surface residence times, and demonstrate that tumbling is the escaping mechanism. For computer simulations to reproduce observations, we use a recent model of R&T [21] in which run times show much larger variability than what would be predicted from a Poisson distribution for the run-to-tumble transitions [22].

Methods.— We implemented 2C-3DT by combining Lagrangian 3D tracking [21, 23] with two-colour fluorescence imaging [24] (See Fig. 1(a)) which are mounted on an inverted epifluorescence microscope (Zeiss-Observer, Z1, C-Apochromat 63×/1.2 W objective). To avoid signal overlap and emission leakage, we engineered an *E. coli* strain (AD62) with body and flagella fluorescence in the green and red respectively (see SI). A two-colour LED

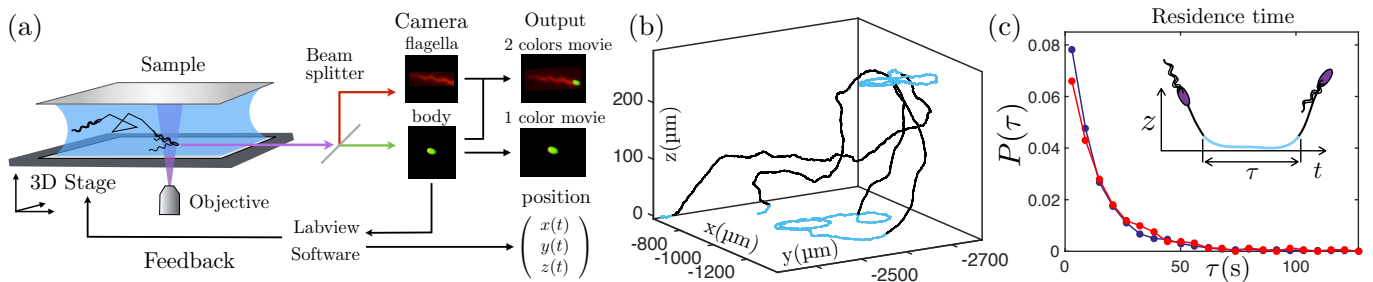


FIG. 1. (a) Sketch of the Lagrangian tracking delivering videos in one or two colours. (b) 3D view of a bacterium trajectory, parts of the trajectory below $8\ \mu\text{m}$ from the surface are in blue. (c) Distribution $P(\tau)$ of residence times τ at the surface. Experimental data are in red and simulations in blue.

light source (Zeiss Colibri 7) and a dichroic filter (Hamamatsu) projected two monochrome images onto different regions of the camera chip. Computer-controlled movement of the microscope stage kept the body of a selected bacterium in focus [23] and images (1024×1024 pixels) are recorded at 80 fps with an Hamamatsu ORCAFlash 4.0,C11440 camera. Green and red images were then superimposed to create a movie of the tracked bacterium and its flagella bundle (see video SI). Photo-bleaching limited flagella imaging to few minutes. For long-time tracking, we use a strain with non-fluorescent flagella (RP437) that allowed one-colour recording of 66 independent cells over 7 h, with the longest track being of $\gtrsim 20$ min duration. Bacteria were grown and prepared using standard protocols [24] (see SI). A $80\ \mu\text{L}$ drop with $\lesssim 3 \times 10^7$ cells mL^{-1} was placed between two glass plates separated by $260\ \mu\text{m}$ and sealed for imaging.

Experimental results.—To measure the surface residence time, τ , Fig. 1(b), we identify when a cell arrives and escapes from a surface. We deem a bacterium to be in the bulk when the body centroid is at $z \gtrsim 8\ \mu\text{m}$ (a typical cell body + flagella length), and arrived at a surface when $z < 3\ \mu\text{m}$. The surface is left again when subsequently, $z \gtrsim 8\ \mu\text{m}$. The residence time τ is defined as the interval between the first and last time a bacterium crosses $z = 3\ \mu\text{m}$. Its value is not influenced by small variations in the choice of these two lengths (see SI).

The measured distribution of surface residence times $P(\tau)$, Fig. 1(c), has mean $\langle \tau \rangle = 21\ \text{s}$ and a long tail extending to a maximum observed τ of $373\ \text{s} \lesssim 20\tau$. These are very long times as compared to the average run time of WT *E. coli* ($\sim 1\ \text{s}$ according to ref.[25]). So, a bacterium typically tumbles more than once during its sojourn at a surface before escaping, apparently confirming the suggestion that tumbling would be an inefficient escape mechanism [20]. The long-tailed, highly-non-exponential, nature of $P(\tau)$ is emphasised when it is plotted against $\ln \tau$, Fig. 2(a), and fitted to a log-normal distribution (exp. $\langle \ln(\tau) \rangle = 2.39\ \text{s}$ and $\sigma = 1.12\ \text{s}$; fit: $\langle \ln(\tau) \rangle = 2.36\ \text{s}$ and $\sigma = 1.16\ \text{s}$).

We measured the incoming and escape angles for cells

arriving (θ_{in}) and leaving (θ_{out}) the surface, defined as: $\theta_{\text{in,out}} = \arcsin(\mathbf{p}_{\text{in,out}} \cdot \mathbf{n})$ where $\mathbf{p}_{\text{in,out}}$ is a unit vector aligned with the body of the bacterium and \mathbf{n} a unit vector normal to the surface. The probability distributions, Fig. 2(b-c), are obtained from 366 pieces of bacterial tracks reaching or leaving the surface. We expect $P(\theta_{\text{in}}) = -\frac{\pi}{180} \sin \theta_{\text{in}} \cos \theta_{\text{in}}$ for cells crossing $z = \delta$ isotropically towards the surface, which agrees with the experimental data shown in Fig. 2(b). Thus the cell incoming angle is not influenced by the surface, in agreement with the observations made using the holographic technique [26].

To understand $P(\theta_{\text{out}})$, we assume a random post-tumble orientation. Then, for a bacterium crossing $z = \delta$ after a tumble at $z = 0$, we expect $P(\theta_{\text{out}}) = \frac{\pi}{180} \cos \theta_{\text{out}}$ if the cell does not tumble before reaching $z = \delta$ [27]. Compared to this expression, our data, Fig. 2(c), show a dip around $\theta_{\text{out}} = 0$ and a peak around 30° . The deficit probably originates in the fact that a cell leaving at a grazing angle ($\theta_{\text{out}} \rightarrow 0$) needs to swim a longer time to reach $z = \delta$, hence maximising its chances for another tumble event *en route*. This will either reorient the cell back to the surface (failed escape) or be logged at $z = \delta$ as escape at a different (likely higher) angle. Finally, the excess of escape at $\theta_{\text{out}} \approx 30^\circ$ indicates hindrance of high-angle tumbles probably due to steric interference from the surface [20].

Next, we characterised the tumbling statistics using 2C-3DT image sequences to identify the tumbling phase unambiguously by identifying the images where at least one flagellum is observed off the flagella bundle. Figure 3(a) shows the trajectory of a typical cell arriving at a surface from the bulk, swimming on the surface before escaping. We manually identify the beginning and end of flagella unbundling by replaying relevant sequences of the two-color movie back and forth. Stills for a typical tumble event are shown in Fig. 3(b) (see SI for video to confirm our identification of the tumbling phase from 0.08 s to 0.83 s). From such analysis, we obtain $P(\tau_t)$, the probability distributions of the bulk and near-wall tumble phase duration compiled from 119 and 241 events

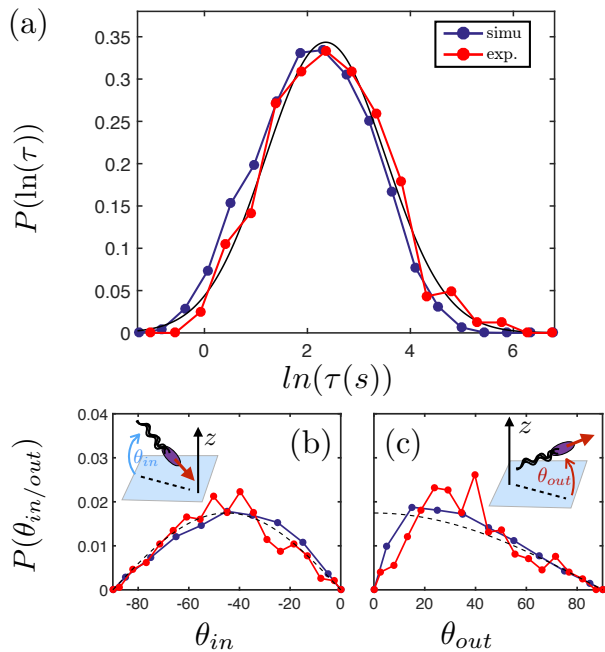


FIG. 2. Comparison between experiment (in red) and simulations (in blue). (a) Distribution of the logarithm of the residence time. The experimental data corresponds to the one on Fig. 1(c), the black line is a Gaussian fit. (b-c) Distributions of the incoming and escape angles out of “single-color” tracking. The black dashed line is the distribution $P(\theta_{in}) = -\frac{\pi}{180} \sin(\theta_{in}) \cos(\theta_{in})$ in (b) and $P(\theta_{out}) = \frac{\pi}{180} \cos(\theta_{out})$ in (c).

respectively, Fig. 3(c). The surface clearly does not affect the tumbling statistics: in each case, $P(\tau_t)$ is peaked around $\tau_t = 0.34$ s with mean $\langle \tau_t \rangle \approx (0.8 \pm 0.1)$ s. Our peaked $P(\tau_t)$ contrasts with a previous report of an exponential distribution [25], which, however, was based on data obtained at the lower rate of 12.6 fps (we work at 80 fps), leading to large uncertainties in the estimated mean of 0.14 ± 0.19 s. This low value is consistent with a more precise recent report of $\langle \tau_t \rangle \approx (0.13 \pm 0.02)$ s [28]. Both studies delimited a tumble event by a sudden dip in swimming speed; this is apparently less sensitive than our direct observation of flagella unbundling, thus giving a lower $\langle \tau_t \rangle$ and giving rise to a peak in $P(\tau_t)$ to below the time resolution of [25]. Although a tumble event does not always lead to an escape, Fig. 3(a), we find that escape is tightly coupled to tumble. Crucially, the distribution of times between an escape event and the previous tumble event, $P(\tau_d)$, is narrowly peaked around zero, Fig. 3(d) [inset], i.e., almost every escape is immediately preceded by a tumble. In contrast, a smooth-swimming strain (CR20) with suppressed tumbling shows residence times longer than our mean observation time of 241 s (see SI). So, contrary to Molaei et al. [20], we find that tumbling is indeed the dominant escape mechanism for a surface-trapped WT *E. coli* cell.

Modelling and computer simulations.— To understand

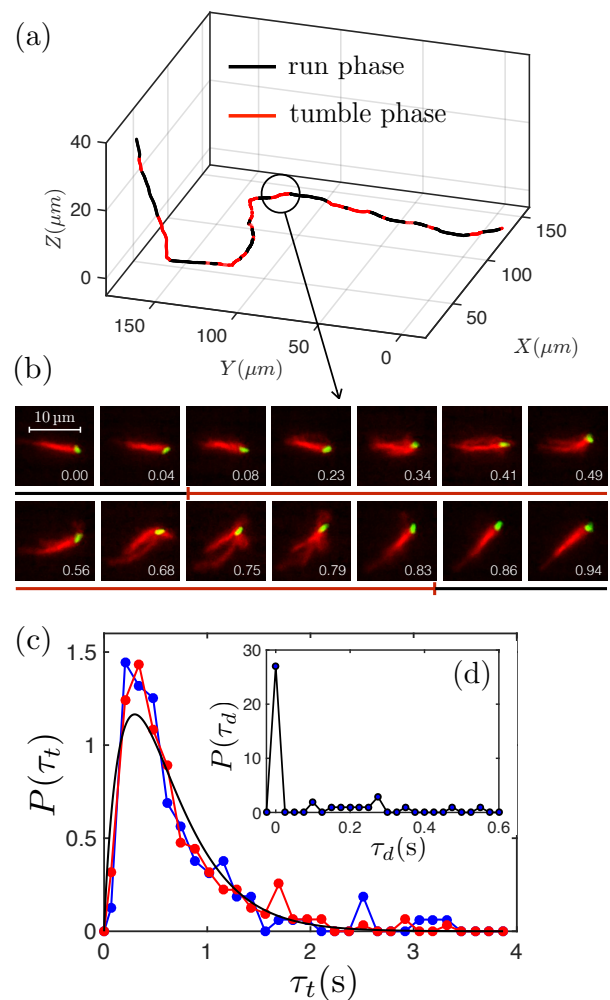


FIG. 3. (a) 3D trajectory of a bacterium (AD62) near the surface, the run phases are in black and the tumble phases in red. (b) Time lapse of a bacterium (strain AD62) during a tumbling event. Each image is overlaid over 3 snapshots. The colour of the line indicates when the tumble starts and ends, it is black for runs and red for the tumble. The total duration of the tumble is 0.71 s. (c) Distribution of tumble duration at surfaces (red) and in the bulk (blue). The black line is a fit using a gamma distribution of parameter $(k, \theta) = (1.9, 0.33)$ s. (d) Distribution of time τ_d between an escape event and the closest previous tumble.

our experimental findings, we turn to simulations. We purposely reduce the complexity of steric, hydrodynamic and other interactions with a surface [4–6, 29] to simple alignment rules. Reorientation due to tumbling is modelled as a rotational diffusion. A particle arriving from the bulk at a surface is supposed align with it. After tumbling, if the orientation points towards the wall, the cell is re-aligned with the surface keeping its vertical position. Otherwise, it leaves the surface with its new orientation. Modelling run and tumble time distributions as a random and uncorrelated Poisson processes with typical values taken from the literature *i.e.* average

run time ≈ 1 s and average tumbling time ≈ 0.1 s [22] does not reproduce the observed $P(\tau)$ as shown in SI. To get quantitative agreement, we implemented a ‘behavioural variability’ (BV) model [21]. The model accounts for an inherent stochasticity borne in the concentration fluctuations of a phosphorylated protein, CheY-P, promoting the switching from counterclockwise to clockwise of the flagella motor rotation. This transition initiates the tumbling process [22, 30]. In the model, the internal parameter δX represents fluctuations in CheY-P concentration around the mean normalised by the standard deviation. Its dynamics is modelled by a Ornstein-Uhlenbeck process leading to a tumbling events rate scaling as $\exp[\Delta_n \delta X]$, where parameter Δ_n is rendering the sensibility of the tumbling process to CheY-P concentration (see model details and parameter choices in SI). We coin this internal time-resolved variable $\delta X(t)$, the swimmer “mood” since for low values, a bacterium will likely run for a long time and explore large distances whereas for larger values it would rather tumble and locally forage.

Trajectories simulated using the BV model show a residence time distribution that matches experiments, Fig. 2(a) without any additional fitting parameter. The simulated distributions of θ_{in} and θ_{out} also quantitatively match the experimental observations, Fig. 2(b-c) and specifically, the small-angle ‘dip’ in $P(\theta_{\text{out}})$. To estimate the extent of this depletion, note that if a bacterium does not reach the escape limit $z = \delta$ before the mean run time $\langle \tau_r \rangle$ ($= 2.32$ s in our model), it will likely tumble. The angle corresponding to a travelling time of $\langle \tau_r \rangle$ over a distance δ at average speed $\bar{v} = 26 \mu\text{m s}^{-1}$ is $\frac{\delta}{\bar{v} \langle \tau_r \rangle} \approx 7.6^\circ$. We therefore expect depletion in $P(\theta_{\text{out}})$ at angles $\lesssim 10^\circ$, as observed. Note, however, that we do not reproduce the small peak in $P(\theta_{\text{out}})$ at $\approx 30^\circ$. We previously interpreted this as an evidence for steric hindrance, an effect not included in the model. Importantly, the same set of model parameters accounts for observations in the bulk or near a wall leading to the conclusion that, on the time scale of our observations, surfaces do not modify significantly the biochemical circuitry controlling tumbling.

From the simulated trajectories, we also obtain the probability distribution of the number of tumbles, N_t , needed before a swimming bacterium trapped at a wall finally escapes, $P(N_t)$, Fig. 4. To understand the exponential behaviour for $N_t \lesssim 10$, we assume that the probability of escape at a single tumble event is p , with no memory of previous tumble events. The probability of escape after N_t events is then $P(N_t) = (1-p)^{N_t-1}p$, or $\log P(N_t) = N_t \log(1-p) + \log\left(\frac{p}{1-p}\right)$. Our data for $N_t \lesssim 10$, Fig. 4, are consistent with $p = \frac{1}{3}$. If all tumbles that reorient a cell away from the surface leads to successful escape, we would rather expect $p = \frac{1}{2}$. It is as if re-orientations into run directions at angles $< \theta_{\text{min}}$ do not lead to escapes, where $\int_{\theta_{\text{min}}}^{\pi/2} \frac{\cos \theta}{2} d\theta = \frac{1}{3}$,

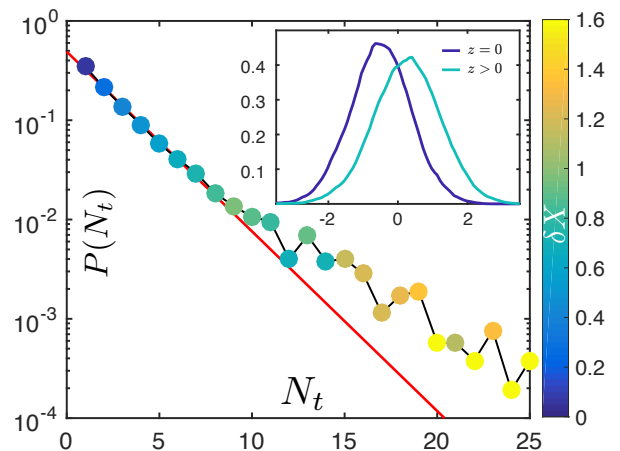


FIG. 4. Distribution of number of tumbles N_t before escape in simulations. The red dashed line plots $P(N_t) = (1-p)^{N_t-1}p$ with $p = \frac{1}{3}$, which gives a mean number of tumbles of $\langle N_t \rangle^* = 2.4$, compared to the mean of the measured distribution $\langle N_t \rangle = 3.5$. Symbol colours show the corresponding dimensionless average CheY-P concentration δX when leaving the surface. Inset: distribution of δX for cells swimming at surfaces (dark blue) and in the bulk (light blue).

or $\theta_{\text{min}} = \arcsin\left(\frac{1}{3}\right) \approx 19^\circ$, which is consistent with the extent of the ‘dip’ in the experimental $P(\theta_{\text{out}})$, Fig. 2(c). The colour of the symbols in Fig. 4 gives the mean δX prior to escape, showing the typical “tumbling mood” when cells leave the surface zone $z < \delta$. The bluish symbols for $N_t \lesssim 10$ indicate that a majority of escaping bacteria are essentially in a long run-time “mood” (or low δX). These bacteria are likely to escape far away from the surface before tumbling again. The simulated $P(N_t)$ displays a large non exponential tail essentially composed by bacteria with large δX . Thus, the short run times of these cells do not lead to efficient escape, because their frequent tumbling increases the probability of being recaptured or remaining at the surface vicinity. The overall implication is that the surface and the bulk display in average, distinct δX distributions: Fig 4 (inset) i.e. surfaces act effectively as a selector for longer-run-time phenotypes.

Summary and conclusions.— Using a novel 2C-3DT method, we measured distributions of sojourn times at a solid surface, incoming and escaping angles and tumbling times, for a wild-type *E. coli*. We found a large distribution of sojourn times as a direct consequence of the bulk run to tumble statistics. However, we found that tumbling is indeed the dominant mechanism by which bacteria escape from surface trapping. Our observations are reproduced quantitatively by a model accounting for stochasticity in the concentration of a protein (CheY-P), which controls the run to tumble statistics. Taken together, our results reveal and explain a paradoxical situation where tumbling appears to be a quite efficient mean to escape from surfaces even though wild-type bacteria

are likely to be trapped in the surface vicinity for times much larger than the typical run time.

Stochasticity in phosphorylated CheY results in ‘behavioral variability’ i.e a time fluctuating ‘tumbling mood’ within a monoclonal population of bacteria. Heterogeneity in bacterial population is usually seen as the consequence of a variety of selection pressures such as ‘bet hedging’ against environmental change [31]. Our findings about surface residence prompts the speculation that behavioural variability in the ‘tumbling mood’ may be a form of bet hedging against planktonic and surface living, allowing at every moment different sub-populations to optimise their behaviour relative to chemotaxis in the bulk [32] and long surface residence leading to biofilm formation. Evaluating this suggestion obviously requires further research to assess precisely the role of internal noise associated with the chemotactic machinery driving the motor rotation in the context of the different possible ‘life styles’ of *E. coli* in their natural habitats.

Acknowledgments.— This work was supported by the ANR grant “BacFlow” ANR-15-CE30-0013, CNRS/Royal Society Grants PHC-1576 and IE160675, and the Institut Pierre-Gilles de Gennes (équipement d’excellence, Investissements d’avenir program ANR-10-EQPX-34). AL and GJ acknowledge support from the ERC Consolidator Grant PaDyFlow under grant agreement 682367. EC is supported by Institut Universitaire de France. VAM, JA, AD and WCKP were funded by ERC (AdG 340877 PHYSAPS).

-
- [1] M. C. Marchetti, J. F. Joanny, S. Ramaswamy, T. B. Liverpool, J. Prost, M. Rao, and R. A. Simha, *Rev. Mod. Phys.* **85**, 1143 (2013).
- [2] H. M. López, J. Gachelin, C. Douarche, H. Auradou, and E. Clément, *Phys. Rev. Lett.* **115**, 028301 (2015).
- [3] V. A. Martinez, E. Clément, J. Arlt, C. Douarche, A. Dawson, J. Schwarz-Linek, A. K. Creppy, V. Škultéty, A. N. Morozov, H. Auradou, and W. C. K. Poon, *Proc. Natl. Acad. Sci. (USA)* **117**, 2326 (2020), <https://www.pnas.org/content/117/5/2326.full.pdf>.
- [4] A. P. Berke, L. Turner, H. C. Berg, and E. Lauga, *Physical Review Letters* **101**, 038102 (2008).
- [5] G. Li and J. X. Tang, *Phys. Rev. Lett.* **103**, 078101 (2009).
- [6] K. Drescher, J. Dunkel, L. H. Cisneros, S. Ganguly, and R. E. Goldstein, *Proc. Natl. Acad. Sci. (USA)* **108**, 10940 (2011).
- [7] E. Perez Ipiña, S. Otte, R. Pontier-Bres, D. Czerucka, and F. Peruani, *Nature Physics* **15**, 610 (2019).
- [8] M. P. Schultz, J. A. Bendick, E. R. Holm, and W. M. Hertel, *Biofouling* **27**, 87 (2011), pMID: 21161774.
- [9] G. D. Bixler and B. Bhushan, *Phil. Trans. R. Soc. A* **370**, 2381 (2012).
- [10] K. Bruellhoff, J. Fiedler, M. Möller, J. Groll, and R. Brenner, *Int J Artif Organs* **33** (2010), doi: 10.1177/039139881003300910. PMID: 20890881.
- [11] G. dong Kang and Y. ming Cao, *Water Research* **46**, 584 (2012).
- [12] C. Marcato-Romain, Y. Pechaud, E. Paul, E. Girbal-Neuhauser, and V. Dossat-Létisse, *Biofouling* **28**, 305 (2012), pMID: 22452390.
- [13] R. M. Wheatley and P. S. Poole, *FEMS Microbiology Reviews* **42**, 448 (2018), <https://academic.oup.com/femsre/article-pdf/42/4/448/25131069/fuy014.pdf>.
- [14] O. E. Petrova and K. Sauer, *J. Bact.* **194**, 2413 (2012), 22389478[pmid].
- [15] H. H. Tuson and D. B. Weibel, *Soft Matter* **9**, 4368 (2013).
- [16] K. Schaar, A. Zöttl, and H. Stark, *Phys. Rev. Lett.* **115**, 038101 (2015).
- [17] P. J. Mears, S. Koirala, C. V. Rao, I. Golding, and Y. R. Chemla, *Elife* **3**, e01916 (2014).
- [18] L. Turner, L. Ping, M. Neubauer, and H. C. Berg, *Biophys. J.* **111**, 630 (2016).
- [19] T. Eisenstecken, J. Hu, and R. G. Winkler, *Soft matter* **12**, 8316 (2016).
- [20] M. Molaei, M. Barry, R. Stocker, and J. Sheng, *Phys. Rev. Lett.* **113**, 068103 (2014).
- [21] N. Figueroa-Morales, R. Soto, G. Junot, T. Darnige, C. Douarche, V. A. Martinez, A. Lindner, and É. Clément, *Phys. Rev. X* **10**, 021004 (2020).
- [22] H. C. Berg, *E. coli In motion* (Springer, New York, 2004).
- [23] T. Darnige, N. Figueroa-Morales, P. Bohec, A. Lindner, and E. Clément, *Rev. Sci. Inst.* **88**, 055106 (2017).
- [24] J. Schwarz-Linek, J. Arlt, A. Jepson, A. Dawson, T. Vissers, D. Miroli, T. Pilizota, V. A. Martinez, and W. C. K. Poon, *Colloids Surf. B* **137**, 2 (2016).
- [25] H. C. Berg and D. A. Brown, *Nature* **239**, 500 (1972).
- [26] S. Bianchi, F. Saglimbeni, and R. Di Leonardo, *Phys. Rev. X* **7**, 011010 (2017).
- [27] A factor of $\sin \theta_{\text{out}}$ such as that appearing in $P(\theta_{\text{in}})$ is not needed because we follow each bacterium from the moment it leaves the surface until it reaches $z = \delta$.
- [28] Z. Qu, F. Z. Temel, R. Henderikx, and K. S. Breuer, *Proc. Natl. Acad. Sci. (USA)* **115**, 1707 (2018).
- [29] E. Lauga, W. R. DiLuzio, G. M. Whitesides, and H. A. Stone, *Biophys. J.* **90**, 400 (2006).
- [30] E. Korobkova, T. Emonet, J. M. Vilar, T. S. Shimizu, and P. Cluzel, *Nature* **428**, 574 (2004).
- [31] I. G. de Jong, P. Haccou, and O. P. Kuipers, *Bioessays* **33**, 215 (2011).
- [32] S. Dev and S. Chatterjee, *Phys. Rev. E* **97**, 032420 (2018).